Research Square

Preprints are preliminary reports that have not undergone peer review.
They should not be considered conclusive, used to inform clinical practice,
or referenced by the media as validated information.

Engineering antiferromagnetic exchange coupling for single-pulse all-optical switching

Yongbing Xu

yongbing.xu@york.ac.uk

University of York

Guanqi Li

Guangdong University of Technology

Jiajun Li

Guangdong Univeristy of Technology

Zihai Li

Guangdong Univeristy of Technology

Wei Xia

Guangdong Univeristy of Technology

Junlin Wang

Guangdong University of Technology https://orcid.org/0000-0002-0383-7864

Jing Wu

Guangdong Univeristy of Technology

Zhendong Chen

Guangdong Univeristy of Technology

Tiejun Zhou

State Key Laboratory of Spintronic Devices and Technologies

Bo Liu

State Key Laboratory of Spintronic Devices and Technologies https://orcid.org/0000-0002-0463-6343

Roy Chantrell

University of York https://orcid.org/0000-0001-5410-5615

Article

Keywords:

Posted Date: April 17th, 2026

DOI: https://doi.org/10.21203/rs.3.rs-9202734/v1

License: This work is licensed under a Creative Commons Attribution 4.0 International License. Read Full License

Additional Declarations: There is **NO** Competing Interest.

Engineering antiferromagnetic exchange coupling for single-pulse all-optical switching

Guanqi Li,[1,†] Jiajun Li,[1,†] Zihai Li,[1] Wei Xia,[1] Junlin Wang,[1,*] Jing Wu,[1,2,*] Xujie Yang,[2] Zhendong Chen,[1,*] Tiejun Zhou[3], Bo Liu[3], Roy Chantrell[1,2] and Yongbing Xu[1,2,4,*]

1. School of Integrated Circuits, Guangdong University of Technology, Guangzhou 510006, China
2. School of Physics, Engineering and Technology, University of York, York, YO10 5DD, United Kingdom
3. State Key Laboratory for Spintronic Devices and Technologies, Hangzhou 311305, China
4. National Key Laboratory of Spintronics, Nanjing University, Suzhou, China

†These authors contributed equally to this work.

*Corresponding authors, E-mail: *junlin.wang@gdut.edu.cn; jing.wu@gdut.edu.cn; chenzd0105@gdut.edu.cn; yongbing.xu@york.ac.uk*

Abstract

Single-pulse all-optical switching (SP-AOS) offers an appealing route to ultrafast magnetic information writing, yet the magnetic parameter that fundamentally determines whether toggle switching occurs has remained unclear. Here we incorporate a Ru spacer into Co/Gd heterostructures to tune the interlayer exchange coupling strength $J_{\mathrm{Gd-Co}}$ through the combined contributions of direct Co–Gd coupling and oscillatory RKKY interactions. The SP-AOS switching signal shows an oscillation nature with the period of Ru thickness less than 1 nm in coincide with the RKKY-defined oscillatory coercive field and saturation magnetization. SP-AOS emerges above a critical antiferromagnetic (AFM) exchange coupling strength of $J_{\mathrm{Gd-Co}} \approx 0.69\mathrm{mJ/m^2}$ and reaches 100% at $J_{\mathrm{Gd-Co}} \approx 1.14\ \mathrm{mJ/m^2}$, where the stronger AFM coupling also lowers the threshold fluence and broadens the operational energy window. Atomistic spin-dynamics simulations further show that the strong $J_{\mathrm{Gd-Co}}$ accelerates the demagnetization dynamics of both Co and Gd sublattices and promotes the formation of the transient ferromagnetic state to enable SP-AOS, whereas weak $J_{\mathrm{Gd-Co}}$ suppresses this transient state and forces the system into a slower, dissipative spin–orbit–driven pathway. These results demonstrate that the key determinant of SP-AOS is not merely associated with the demagnetization times of the two sublattices, but is directly linked to the strength of antiferromagnetic exchange coupling. This study establishes the antiferromagnetic exchange coupling strength as a practical and designable criterion for nanoscale materials engineering of ultrafast photomagnetic switching.

Introduction

SP-AOS has emerged as a key candidate mechanism for ultrafast magnetic writing[1,2] because it requires no external magnetic field while offering both ultrafast speed[3,4] and ultralow energy consumption[5]. Although all-optical switching has been observed in a broad range of materials[6-11], only a very limited number of systems have been shown to support SP-AOS, and the material criterion governing its occurrence remains unclear. To date, SP-AOS has been realized mainly in rare-earth–transition-metal ferrimagnetic alloys or multilayers[12-15], Mn_2Ru_xGa[16], and the spin-valve structure Pt/Co/Cu/Co/Pt[17]. Excluding Pt/Co/Cu/Co/Pt, the former two classes, despite their distinct compositions, share a common ultrafast dynamical basis: they consist of two antiparallel magnetic sublattices that, under ultrafast laser heating, develop a transient ferromagnetic-like state owing to their unequal demagnetization rates, ultimately driving single-pulse all-optical switching[18,19]. This indicates that the essential requirement for SP-AOS is not laser-induced demagnetization itself[20], but whether sufficiently efficient angular momentum transfer can be established between antiparallel sublattices on the ultrafast timescale to generate the transient ferromagnetic-like state required for switching.

This question directly points to the angular momentum transfer mechanisms specific to antiferromagnetic and ferrimagnetic systems. Unlike ferromagnets, where angular momentum transfer is governed primarily by spin–lattice dissipation mediated by spin–orbit coupling[21,22], antiferromagnetic and ferrimagnetic materials possess an additional transfer channel mediated by direct exchange interaction between antiparallel sublattices[23-25]. Because this channel is faster and less dissipative, it is widely regarded as the core dynamical basis of SP-AOS. Previous studies have further shown that the angular momentum transfer rate itself determines whether AOS can occur: once this process is slowed, systems that originally exhibit single-pulse switching are driven into a non-switching state[26]. Nevertheless, direct experimental evidence identifying the key material parameter that governs this transfer rate remains lacking. In particular, how the inter-sublattice antiferromagnetic exchange strength controls angular momentum transfer efficiency, and thereby determines the onset, energy threshold and deterministic character of SP-AOS, remains a central open question in the field.

To directly test the role of antiferromagnetic exchange in SP-AOS, we constructed an artificial ferrimagnetic heterostructure, Co/Ru(x)/Gd, in which the inter-sublattice exchange interaction can be continuously tuned. By varying the Ru spacer thickness, we engineer the competition between direct Co–Gd exchange and oscillatory RKKY interaction[27-30], thereby continuously controlling the effective inter-sublattice antiferromagnetic exchange coupling strength. Combining magneto-optical Kerr

microscopy, vibrating sample magnetometry and X-ray magnetic circular dichroism measurements, we show that antiferromagnetic exchange coupling strength is the key quantitative parameter governing whether SP-AOS occurs, as well as its switching ratio and energy threshold. Both the experimental and simulation results reveal that sufficiently strong inter-sublattice antiferromagnetic exchange coupling is a prerequisite for SP-AOS, where strong AFM coupling promotes rapid angular momentum transfer between the sublattices and thus the SP-AOS, and weak AFM coupling instead drives the system into a slower and more dissipative spin–orbit–lattice channel, thereby suppressing single-pulse switching.

Results and Discussion

(1) Engineering tunable inter-sublattice exchange in Co/Ru(x)/Gd

We fabricated Glass/Ta (4 nm)/Pt (4 nm)/Co (1.5 nm)/Ru (x nm)/Gd (3 nm)/Pt (2 nm) multilayers by magnetron sputtering with systematically varied Ru thickness, as illustrated in Fig. 1a. The Pt underlayer induces perpendicular magnetic anisotropy (PMA) through strong interfacial spin–orbit coupling (SOC). When Co and Gd are in direct contact, their moments align antiparallel through an indirect 3d–5d–4f exchange pathway: Co 3d electrons couple antiferromagnetically to Gd 5d6s states, while strong Hund's coupling within Gd aligns the 5d6s and 4f moments parallel to each other, resulting in a net antiferromagnetic Co–Gd interaction.

Inserting a Ru spacer substantially modifies this interaction. Ru 4d conduction electrons mediate an oscillatory RKKY-type exchange between the Co and Gd layers. On the Co side, 3d electrons polarize the Ru 4d states, whereas on the Gd side, the delocalized 5d–6s electrons, aligned with the localized 4f moments, hybridize with Ru. This establishes an indirect Co–3d ↔ Ru–4d ↔ Gd–5d ↔ Gd–4f exchange pathway, producing alternating ferromagnetic and antiferromagnetic coupling as a function of Ru thickness, as schematically illustrated in Fig. 1b. Transmission electron microscopy and X-ray diffraction measurements (Supplementary Section 1) further reveal interfacial intermixing between Gd and Ru. As a result, the direct Co–Gd exchange and the Ru-mediated indirect exchange can coexist, leading to either enhancement or reduction of the net antiferromagnetic Co–Gd coupling depending on their relative contributions.

To quantify this tunability, we performed density functional theory (DFT) calculations of the Co–Gd exchange energy as a function of Ru thickness using the Vienna ab initio simulation package (VASP)[31,32]. The calculated exchange exhibits a pronounced oscillation, including a sign reversal at several monolayers (Supplementary Fig. S2), demonstrating that inserting Ru enables continuous control of both the magnitude and sign of the interlayer coupling.

Because ultrathin Gd has a Curie temperature below room temperature[33,34], its magnetic moment in our samples is exchange-induced by the adjacent Co layer. Therefore, stronger AFM coupling produces a larger antiparallel Gd moment, increasing the coercive field and reducing the net saturation magnetization, whereas weaker coupling has the opposite effect, as illustrated schematically in Fig. 1c. Vibrating Sample Magnetometer (VSM) measurements provide direct experimental validation of this scenario. As shown in Fig. 1d, the hysteresis loops of Co(1.5 nm)/Ru(x)/Gd(3 nm) (red) differ markedly from that of the reference Pt/Co(1.5 nm)/Pt sample (blue) and evolve systematically with Ru thickness. Both the saturation magnetization and the coercive field exhibit clear oscillatory behavior as a function of Ru thickness, unambiguously demonstrating that the Co–Gd interlayer coupling is periodically modulated by the inserted Ru spacer. Notably, three samples with Ru thicknesses of 0, 0.8, and 1.5 nm exhibit a significantly reduced saturation magnetization and an enhanced coercive field compared to others, indicating a relatively strong antiferromagnetic coupling between Co and Gd. These samples are highlighted with a yellow background in Fig. 1d.

To directly probe the Gd magnetic moment, we performed element-specific X-ray Magnetic Circular Dichroism (XMCD) measurements at the Gd M_4 and M_5 absorption edges. Consistent with the VSM results, the XMCD intensity varies strongly with Ru thickness (Supplementary Fig. S3). For the sample with x=0.2 nm, the XMCD signal is nearly absent, indicating that the Gd layer remains essentially unpolarized at room temperature. At this thickness, DFT predicts that the Co–Gd exchange is nearly quenched, and the measured saturation magnetization is nearly identical to that of the Pt/Co/Pt reference sample, further confirming that Gd carries little to no induced moment when the exchange field from Co is negligible. This behavior directly reflects the paramagnetic nature of ultrathin Gd in the absence of Co-mediated exchange coupling.

In contrast, the directly contacted Co/Gd sample ($x = 0$ nm) exhibits clear XMCD signals at both absorption edges, demonstrating that strong antiferromagnetic exchange induces a substantial Gd moment antiparallel to Co. Even more strikingly, when the Ru spacer thickness is tuned to $x \approx 0.8$ nm, the XMCD intensity exceeds that of the direct-contact bilayer ($x = 0$ nm). This enhancement coincides with the minimum M_S and maximum H_c observed in Fig. 1d, indicating that the AFM coupling reaches its strongest value at this Ru thickness.

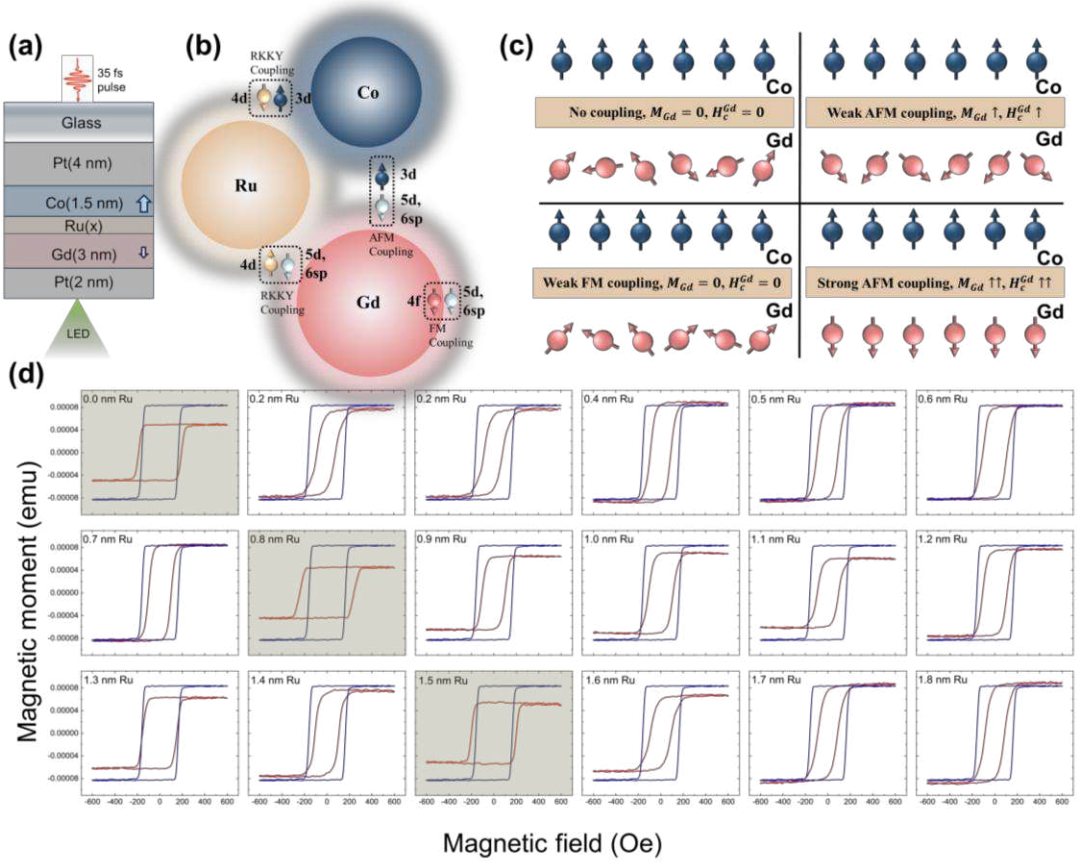


Figure 1 | Structure, interfacial exchange mechanisms, and Ru-dependent magnetic properties of Pt/Co/Ru/Gd/Pt multilayers. (a) Schematic of the multilayer architecture and experimental geometry used to probe SP-AOS in Glass/Ta (5 nm)/Pt (4 nm)/Co (1.5 nm)/Ru(x)/Gd (3 nm)/Pt (2 nm) stacks. **(b)** Illustration of the competing interfacial exchange pathways. The itinerant Gd 5d–6sp electrons couple antiferromagnetically to Co 3d states, while aligning ferromagnetically with the localized Gd 4f moments, producing an overall AFM Co–Gd interaction. Both sublattices additionally couple to the Ru spacer via the oscillatory RKKY mechanism, which alternates between FM and AFM character as a function of Ru thickness. **(c)**, Schematic representation of the induced Gd magnetic moment and coercive field under different Co–Gd coupling regimes. Without coupling, the Gd layer exhibits neither a net moment nor coercive field. Weak FM or AFM coupling yields a small induced moment and modest coercive field, whereas strong AFM coupling produces a large induced Gd moment accompanied by pronounced coercive field. **(d)**, VSM measurements of all samples. The numbers in the figure denote the Ru spacer thickness in nanometers. The blue line represents the VSM result of the reference sample, Pt/Co (1.5 nm)/Pt. The three samples highlighted with a yellow background exhibit saturation magnetization that are significantly smaller than those of the reference sample.

Together, the XMCD, VSM and DFT results provide direct and mutually consistent evidence that the induced Gd moment, and hence the effective Co–Gd exchange coupling, oscillates strongly with Ru thickness. This tunable inter-sublattice antiferromagnetic exchange establishes Co/Ru(x)/Gd as a model artificial ferrimagnetic platform for investigating the role of exchange coupling in single-pulse all-optical switching.

(2) Ru-thickness-dependent emergence of SP-AOS

To systematically investigate SP-AOS, we performed measurements on samples with varying Ru spacer thickness. Two types of experiments were conducted: (i) energy-dependent measurements excited by a single pulse with the pulse energy varied from 7.5 to 18 nJ in order to determine the switching threshold and switched area, and (ii) toggle-switching tests excited by five consecutive laser pulses with a fixed pulse energy of 15.5 nJ. All measurements were performed using a wide-field MOKE microscope, which allows direct visualization of the magnetization patterns before and after laser illumination. The samples are initially magnetized as a dark magnetic contrast. The switching ratio was obtained by quantifying the fraction of reversed pixels within the illuminated area (see Supplementary Section 5 for details).

We first examined the energy-threshold behavior of samples with different Ru spacer thicknesses using a single-pulse excitation with various laser fluence, as summarized in Fig. 2a. The response to laser excitation varies markedly with Ru thickness. At a relatively low pulse energy of 7.5 nJ, clear magnetization reversal is observed only in a subset of samples with stronger AFM coupling, and the switched area increases with the coupling strength. In particular, the sample with $x = 0.8$ nm exhibits a well-defined largest reversed region after single-pulse excitation, whereas samples with weaker AFM coupling—such as those with $x = 0.2$ nm, 0.3 nm, or 1.6–1.8 nm—show almost no detectable changes in magnetic contrast.

When the pulse energy is increased to 10 nJ, laser-induced magnetic modifications become visible in all samples, yet the switched area still exhibits a pronounced dependence on Ru thickness. Overall, as the Co–Gd exchange varies with Ru thickness, the area affected by a single pulse shows a strong non-monotonic trend: samples with stronger antiferromagnetic coupling display larger and more coherent reversed regions, while those with weaker coupling exhibit only localized demagnetization or fragmented domain patterns near the center of the laser spot. As the pulse energy is further increased to 13–18 nJ, the same trend persists: weakly coupled samples tend to develop irregular, thermally induced multidomain structures, whereas strongly coupled samples continue to show more uniform AOS behavior.

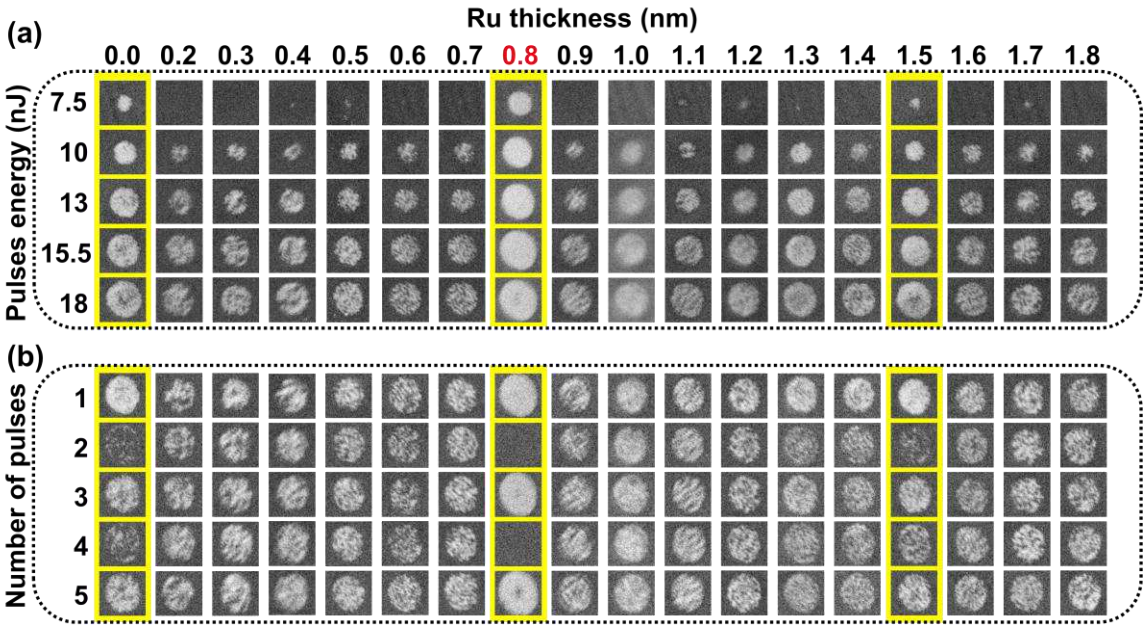


Figure 2 | MOKE images of AOS in Pt/Co/Ru/Gd/Pt multilayers. Each image has a side length of 26 μm. (a) AOS Switching excited by a single pulse with pulse energies of 7.5, 10, 13, 15.5 and 18 nJ (3.32~8 mJ/cm^2), illustrating the strong Ru-thickness dependence of the switched area and the AOS threshold. **(b)** Toggle-switching behavior excited by five consecutive pulses at a pulse energy of 15.5 nJ (6.88 mJ/cm^2), showing 100% toggle reversal only at Ru $\approx 0.8\,nm$. The three samples highlighted with a yellow background are identical to those marked in Fig. 1d. Notably, these samples exhibit substantially improved AOS performance compared to the remaining samples.

Under a fixed pulse energy of 15.5 nJ, the magnetization reversal behavior excited by five consecutive laser pulses shows a strong dependence on the Ru thickness, as summarized in Fig. 2b. For the sample with $x = 0.2$ nm, where the Co–Gd exchange is nearly quenched, the magnetic contrast shows a multidomain state after the 1st laser pulse excitation and stays almost the same for the rest four pulses' exposure. This is consistent with the nearly vanishing Gd XMCD signal and with the saturation magnetization M_s being nearly identical to that of the Pt/Co/Pt reference sample, indicating that the Gd layer remains unpolarized at room temperature.

For the directly contacted Co/Gd structure ($x = 0$ nm), the 1st pulse induces approximately 92% reversal within the illuminated region; however, the second pulse fails to restore the initial uniform state and instead produces a multidomain pattern. This behavior is consistent with earlier reports showing that SP-AOS is suppressed once the Co thickness exceeds ~1.4 nm[14,35]. In our design, the Co layer thickness was intentionally chosen as 1.5 nm, which explains the absence of

reversible toggle switching in this sample despite its relatively high single-pulse switching ratio.

At a Ru thickness of $x \approx 0.8$ nm, the SP-AOS response becomes most pronounced: the 1st pulse induces nearly complete magnetization reversal, and subsequent pulses reliably toggle the magnetization between opposite states. As the Ru thickness increases to 1.3 and 1.5 nm, the switching behavior weakens, and at $x = 1.1$ nm the toggle response disappears entirely. Samples that exhibit ferromagnetic interlayer coupling show no observable AOS under the same excitation conditions. These observations indicate that the emergence of SP-AOS is governed not simply by Ru thickness itself, but by the effective inter-sublattice antiferromagnetic exchange strength tuned by Ru insertion.

(3). Antiferromagnetic exchange strength quantitatively governs SP-AOS

We summarize the coercive field, saturation magnetization, and the Kerr signal after one laser pulse for all samples in Fig. 3a–c. Notably, all three quantities exhibit remarkably similar trends as functions of Ru thickness. Figures 3a and 3b show clear oscillatory behavior in both coercive field and saturation magnetization, with a period below 1 nm, consistent with the characteristic thickness dependence of RKKY-mediated interlayer exchange coupling[36-38]. Importantly, the Kerr signal after a single laser pulse in Fig. 3c follows the same oscillatory trend. Samples with larger coercivity and lower saturation magnetization, both signatures of stronger antiferromagnetic Co–Gd coupling, exhibit a much stronger SP-AOS response. This close correspondence establishes that the Ru-thickness-dependent AOS behavior is directly linked to the oscillatory evolution of the Co–Gd exchange interaction.

Here, the Ru thickness itself is merely a structural tuning parameter; its essential role is to modify the AFM exchange interaction between the Co and Gd layers. To uncover the universal trend underlying the observed AOS behavior, we go beyond the specific sample structural description and analyze the data in terms of the underlying physical control parameter—the Co–Gd AFM exchange coupling strength.

Because thin-film Gd has a Curie temperature far below room temperature, it does not exhibit spontaneous magnetization at ambient conditions; its effective magnetic moment arises entirely from exchange coupling with the Co layer[39]. At room temperature, the Gd layer can thus be regarded as a paramagnetic subsystem characterized by a magnetic susceptibility χ_{Gd}, while the interaction term $J_{\mathrm{Gd-Co}} M_{\mathrm{Co}}(T)$ acts as an effective exchange field H_{ex} exerted by Co. Within a mean-field description, the induced Gd moment can be written as[40,41]:

$$M_{\mathrm{Gd}}(T) \approx \chi_{\mathrm{Gd}}(T) H_{\mathrm{ex}} \propto \chi_{\mathrm{Gd}}(T) J_{\mathrm{Gd-Co}} M_{\mathrm{Co}}(T),$$

indicating that the induced Gd moment at room temperature provides a quantitative indicator of the effective Co–Gd AFM exchange strength.

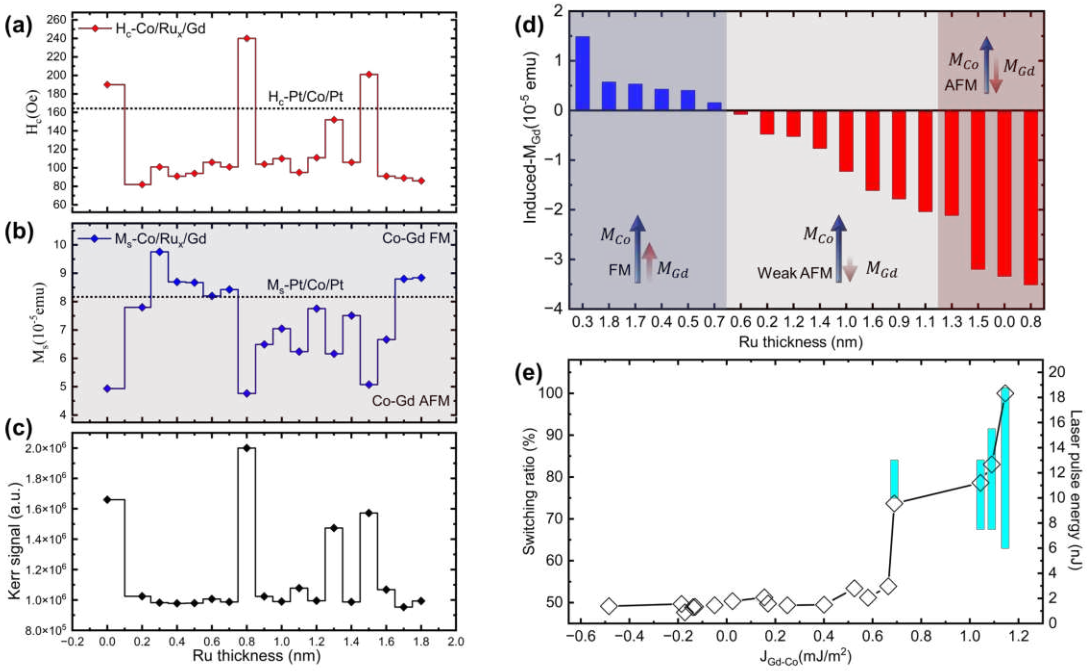


Figure 3 | Ru-thickness-dependent magnetic properties and SP-AOS performance. (a, b) Coercive field H_c and Saturation magnetization M_s extracted from VSM measurements. The dashed line indicates the H_c and M_s of the reference sample. **(c)** Ru-thickness dependence of the Kerr signal after one laser pulse. **(d)** Induced Gd magnetic moment M_{Gd} for samples with different Ru spacer thicknesses. The samples are reordered according to the magnitude of M_{Gd}, which quantitatively reflects the Co–Gd AFM exchange strength; thus, the horizontal axis does not follow the monotonic Ru-thickness sequence. **(e)** SP-AOS switching ratio and energy window (shown as blue bars) as a function of $J_{\mathrm{Gd\text{-}Co}}$.

To quantify the exchange-induced Gd moment, we fabricated a Pt/Co/Pt reference sample with an identical Co thickness but without Ru or Gd. The magnetic moment of this reference represents the intrinsic contribution from the Co layer. By subtracting this intrinsic Co moment from the total magnetization of each Ru–Gd–containing multilayer, we extract the exchange-induced Gd moment, which provides a quantitative indicator of the effective interlayer Co–Gd coupling strength and allows us to extract $J_{\mathrm{Gd-Co}}$. When the samples are reordered according to the magnitude of the induced Gd moment—that is, by their effective AFM coupling strength—the corresponding trend is presented in Fig. 3d. Accordingly, in Fig. 3d the samples are arranged by the magnitude of the extracted Gd moment rather than by increasing Ru

thickness, which is why the Ru-thickness axis appears out of sequence. As discussed above, the sign and magnitude of the extracted Gd moment reflect the nature and strength of the effective Co–Gd exchange coupling. In our sign convention, a positive extracted Gd moment corresponds to effective FM coupling between Co and Gd, whereas a negative value corresponds to effective AFM coupling; a larger negative magnitude indicates stronger AFM exchange. Based on the extracted Gd moments, we therefore classify the samples into three distinct regimes: ferromagnetic coupling, weak antiferromagnetic coupling, and strong antiferromagnetic coupling as shown in Fig. 3d.

Using the extracted Gd moment, we converted the effective Co–Gd interlayer coupling into $J_{\mathrm{Gd-Co}}$, and further replotted the SP-AOS switching ratio and the single-pulse switching threshold as functions of $J_{\mathrm{Gd-Co}}$, as shown in Fig. 3e. This representation reveals a clear trend: the occurrence and performance of SP-AOS are not determined directly by Ru thickness itself, but are instead governed by the antiferromagnetic exchange strength between the Co and Gd sublattices.

First, the switching ratio of SP-AOS increases markedly with increasing antiferromagnetic exchange strength. In the ferromagnetic and weak-antiferromagnetic regimes, the switching ratio remains low, at around 50%, indicating that laser excitation drives the system mainly into a multidomain demagnetized state rather than a well-defined final magnetic state. As $J_{\mathrm{Gd-Co}}$ increases to approximately 0.69 mJ/m^2, the switching ratio rises sharply, indicating that the system crosses the critical exchange strength required for SP-AOS. When $J_{\mathrm{Gd-Co}}$ further increases to about 1.14 mJ/m^2, the switching ratio reaches 100%.

Second, strengthening the antiferromagnetic exchange does not raise the switching threshold of SP-AOS; instead, it lowers the required laser energy significantly. Experimentally, the sample with the strongest Co–Gd antiferromagnetic exchange exhibits the lowest SP-AOS threshold, with a threshold fluence of 1.8 mJ/cm^2. This result indicates that strong antiferromagnetic coupling facilitates more efficient angular momentum transfer between the two antiparallel sublattices, thereby enabling switching at substantially lower optical excitation energy.

Furthermore, strong antiferromagnetic exchange also significantly broadens the operational energy window for SP-AOS. When the exchange strength is about 0.69 mJ/m^2, SP-AOS is sustained only within a narrow pulse-energy range of 10–13 nJ. When the exchange strength is further increased to 1.14 mJ/m^2, this range broadens substantially to 6–18.75 nJ, as indicated by the blue bars in Fig. 3e. This means that strong antiferromagnetic exchange not only makes SP-AOS easier to trigger, but also markedly improves its tolerance to laser-energy fluctuations, thereby enhancing the

experimental robustness of single-pulse all-optical switching and its potential for device applications.

Taken together, Fig. 3e shows that the antiferromagnetic exchange strength between the Co and Gd sublattices is the key quantitative parameter determining whether SP-AOS occurs, whether the switching is deterministic, as well as the switching threshold and the width of the operational window. These results demonstrate that a sufficiently strong inter-sublattice AFM exchange is required for SP-AOS.

(4) Strong exchange enables rapid angular-momentum transfer and transient ferromagnetic-state formation

To further elucidate how the Co–Gd AFM exchange strength governs ultrafast spin dynamics and the conditions required for SP-AOS, we performed atomistic spin-model simulations following the methodology of Ostler *et al.*[42]. By applying the same laser excitation to systems with different AFM coupling strengths, we directly compared the demagnetization behavior and transient magnetic-state evolution across strongly and weakly coupled samples on femtosecond timescales, thereby quantifying how the coupling strength influences the magnetization-reversal process.

The simulation results reveal that the AFM exchange strength has a decisive impact on the spin dynamics of the Co–Gd system. As shown in Fig. 4a, at 100% AFM coupling, the Co magnetization rapidly decreases after laser excitation and crosses zero at ~4 ps, producing a transient ferromagnetic state and enabling SP-AOS. When the AFM coupling is reduced to 60%, the Co demagnetization becomes slower, and the transient ferromagnetic state emerges only after ~5 ps (Fig. 4b). Further decreasing the coupling to 20% results in even slower demagnetization with insufficient amplitude; under these conditions, the Co magnetization never reaches zero and no transient ferromagnetic state forms, rendering SP-AOS impossible (Fig. 4c). The dependence of the demagnetization dynamics on AFM coupling is summarized in Fig. 4d and 4e, which clearly demonstrate that the demagnetization rate of both Co and interfacial Gd is positively correlated with the Co–Gd exchange strength.

These observations can be understood in terms of two competing channels for angular-momentum transfer. In conventional ferromagnets, ultrafast demagnetization proceeds primarily through a spin–orbit–mediated pathway: spin angular momentum is first transferred to the orbital sector and subsequently dissipated into the lattice. Extensive TR-XMCD[21] and femtosecond X-ray diffraction[22] studies on 3d ferromagnets have shown that this pathway is highly dissipative and typically accompanied by pronounced precessional dynamics. In contrast, antiferromagnetically coupled antiferro/ferri-magnets possess an additional, fundamentally different channel in which angular momentum can be redistributed

directly between the two antiparallel sublattices without first coupling to the lattice [23-25,43].

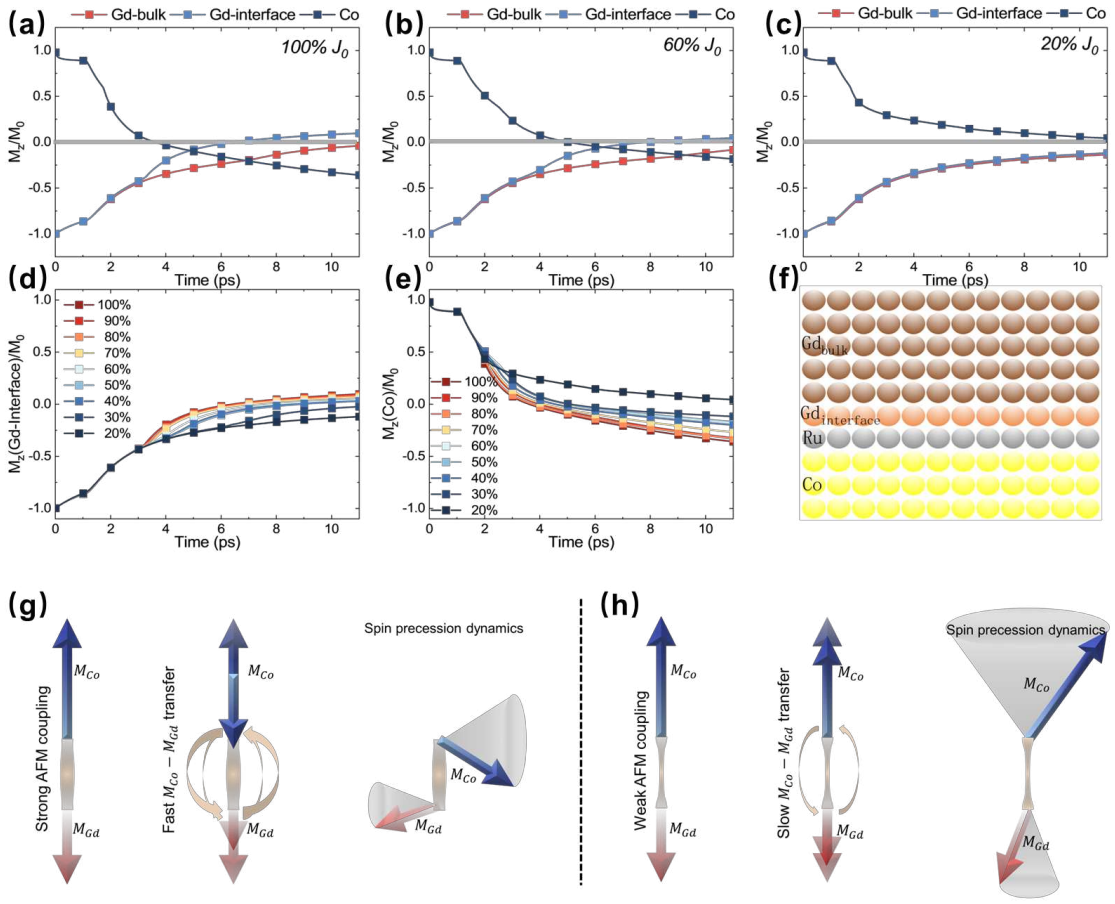


Figure 4 | Atomistic spin-dynamics simulations revealing the role of interlayer AFM exchange in SP-AOS. (a-c) Ultrafast spin dynamics in Co/Ru/Gd multilayers with 100%, 60%, and 20% AFM coupling. Strong coupling enables rapid Co–Gd angular-momentum transfer and cooperative reversal, while weak coupling suppresses it. **(d, e)** Demagnetization times of interfacial Gd and Co decrease monotonically with increasing AFM coupling strength. **(f)** Atomistic spin model including Co, Ru, interfacial Gd, and bulk Gd layers. **(g, h)** Spin-dynamics trajectories for strong and weak AFM coupling, illustrating transient-ferromagnetic reversal versus precession demagnetization.

By tuning the Co–Gd AFM exchange strength, our simulations reveal how the balance between these two channels evolves. When the coupling is strong, the exchange-mediated inter-sublattice transfer dominates, allowing angular momentum to be rapidly exchanged between Gd and Co. This enables the Co moments to reverse within ~4 ps and stabilizes the transient ferromagnetic state required for SP-AOS. When the

AFM coupling is weak, however, the exchange-mediated channel becomes inefficient, forcing the system to rely on the slower and more dissipative SOC-mediated pathway, which cannot support the formation of a transient ferromagnetic state. The monotonic decrease in the demagnetization times of Co and Gd with increasing coupling strength (Fig. 4d, e) quantitatively links the demagnetization rate to the underlying AFM exchange interaction.

More broadly, AFM-coupled systems intrinsically host two angular-momentum-transfer pathways: (1) a direct, exchange-mediated channel between antiparallel sublattices—unique to AFM order; and (2) a SOC-driven spin → orbital → lattice channel, analogous to that in ferromagnets. The relative dominance of these two pathways is determined entirely by the Co–Gd exchange strength. Strong AFM coupling favors fast, low-dissipation angular-momentum redistribution between sublattices, whereas weak coupling shifts the system toward a ferromagnet-like regime dominated by precessional and dissipative dynamics. Consequently, enhancing AFM exchange not only accelerates ultrafast demagnetization but also reduces the energy required for magnetic reversal by circumventing the highly dissipative spin–orbit–lattice transfer process—providing a clear microscopic basis for the high efficiency and low threshold of SP-AOS.

By systematically tuning the AFM exchange coupling between Co and Gd, this work addresses a longstanding central question in the study of SP-AOS: why do many materials that possess antiferromagnetic coupling and distinct sublattice demagnetization times still fail to exhibit SP-AOS? We find that having two demagnetization timescales, while necessary, is not sufficient to trigger single-pulse magnetization reversal; the decisive parameter is the strength of the AFM exchange between the sublattices. The continuously tunable coupling enabled by varying the Ru spacer thickness allows us to experimentally establish a one-to-one correspondence between the SP-AOS switching ratio, the energy threshold, and the AFM exchange strength, thereby identifying AFM coupling as the key control parameter for SP-AOS.

In conclusion, this work establishes antiferromagnetic-exchange engineering as a materials design principle for achieving SP-AOS. By continuously tuning the interlayer exchange interaction in a synthetic ferrimagnetic Co/Ru/Gd heterostructure, we demonstrate a direct and quantitative correlation between exchange strength and switching performance, including the switching ratio, threshold fluence and operational energy window. SP-AOS emerges only after the inter-sublattice AFM exchange coupling strength exceeds a critical value; and the strong AFM coupling rises the switching ratio, decreases threshold fluence and expands the operational pulse-energy window.

Beyond identifying a decisive physical parameter, our results reveal how exchange engineering reshapes ultrafast spin dynamics at the materials level. Strong antiferromagnetic coupling promotes rapid and low-dissipation angular-momentum transfer between antiparallel sublattices, enabling formation of the transient ferromagnetic-like state required for SP-AOS. By contrast, weak coupling drives the system into a slower and more dissipative spin–orbit–lattice pathway that suppresses single-pulse reversal. This framework should extend beyond the specific Co/Ru/Gd system studied here. The same ultrafast switching pathway could in principle be applied to other heterostructures, where inter-sublattice exchange can be independently engineered through spacer selection, thickness control or interface design. Antiferromagnetic-exchange engineering therefore provides a general and practical strategy for designing ultrafast, energy-efficient photomagnetic and spintronic materials.

Materials and Methods

1. Sample preparation

Multilayer stacks with the structure Glass/Ta (5 nm)/Pt (4 nm)/Co (1.5 nm)/Ru (x nm)/Gd (3 nm)/Pt (2 nm) were fabricated by DC magnetron sputtering at room temperature. Commercial Corning glass substrates (thickness ≈ 0.13 mm) were used to enable optical transmission for magneto-optical Kerr effect (MOKE) imaging in a back-illumination geometry. A 5 nm Ta buffer layer was first deposited to improve surface flatness and promote the (111) texture of the subsequent Pt layer. The 4 nm Pt underlayer, with its strong spin–orbit coupling, enhances perpendicular magnetic anisotropy (PMA) at the Pt/Co interface. A 2 nm Pt capping layer was also added to prevent oxidation of the Gd layer while ensuring adequate XMCD signal strength. During deposition, the base pressure was better than 5×10^{-8} Torr, and the Ar working pressure was approximately 2×10^{-3} Torr. All sputtering powers were optimized to achieve accurate thickness control. The Ru spacer thickness was systematically varied between 0 and 1.8 nm. The deposition rates were calibrated as follows: Ta – 0.33 Å/s, Pt – 0.13 Å/s, Co – 0.08 Å/s, Ru – 0.17 Å/s, and Gd – 0.24 Å/s. All films were grown without substrate heating to minimize interdiffusion at the Ru/Gd interface.

2. Single-pulse all-optical switching experiments

A schematic of the optical setup is shown in Fig. S5. The excitation source was a Ti:sapphire femtosecond laser (central wavelength 800 nm, pulse duration 35 fs). The laser fluence was continuously adjusted by a pair of polarizers with a rotatable half-wave plate in between. The beam was then focused onto the sample surface by a 10 cm focal-length lens, yielding a spot diameter of approximately 24 μm. The laser was

normally incident on the film plane. The use of transparent glass substrates allowed transmission MOKE imaging, enabling visualization of the magnetization reversal process in real time. The transmitted probe light was collected by a second lens, passed through an analyzing polarizer, and recorded by a CMOS camera. For uniform illumination, an LED light source was collimated and coupled into the optical path through an additional polarizer. A pair of permanent magnets provided an external bias field to initialize the magnetic state prior to laser excitation.

3. Atomistic Spin Model

The atomistic spin model, combined with the two-temperature model [44], is employed within the Vampire package to simulate ultrafast laser-induced magnetization dynamics in a Pt/Co/Ru(x)/Gd synthetic antiferromagnetic multilayer. The system's energetics are governed by a spin Hamiltonian of the form:

$$H = -\sum_{i<j} J_{ij}\, S_i \cdot S_j - \sum_i k_u S_i^z - \sum_i \mu_i\, S_i^z B^z$$

Here, $S_{i,j}$ are unit vectors representing the spin directions, J_{ij} is the exchange energy between atoms i, j, $k_u$is the uniaxial anisotropy on the Co and Gd sites, and B^z is the externally applied magnetic field. The simulated structure consists of a 0.5 nm thick Co layer, a 0.16 nm Gd interface layer, and a 0.84 nm Gd bulk layer. The antiferromagnetic coupling strength between the Co and Gd layers is controlled by the variable thickness x of the Ru spacer layer. The interlayer RKKY interaction strength $J_{Co\text{-}Gd}$ is set as -1.09^{-21}J/Link, the $J_{Co\text{-}Co}$ is 5.9×10^{-21}J/Link and the $J_{Gd\text{-}Gd}$ is 1.26×10^{-21}J/Link. The magnetic moment of Co and Gd are set as 1.61 μB and 7.63 μB. The perpendicular magnetic anisotropy of Co layer is set as 3.73×10^{-23}J, and for the Gd layer is 8.03×10^{-23}J. The laser pulse duration is 35 fs with power as 45 [45]. The damping parameters are set to 0.1 for the Co layer and 0.05 for the Gd layer. The system is initially equilibrated at 300 K for 1 ps before the laser pulse is applied.

Supplementary material

Supplementary material is available from the *Nature Nanotechnology* or from the author.

Acknowledgements

This work was supported by the National Natural Science Foundation of China (Grant Nos. 12241403, 12304136, T2394474, 62104196, and 12404128), National Key Research and Development Program of China (Grant Nos. 2020YFA0309300, 2023YFF0719200, and 2024YFA1408801), “Chunhui” international cooperation

Program (Grant No. HZKY20220018), Guangdong Basic and Applied Basic Research Foundation (Grant Nos. 2022A1515110863 and 2023A1515010837), Guangdong Science and Technology Project (Grant No. 2023QN10X275), Natural Science Foundation of Guangdong (No. 2024A1515012039), and Project for Maiden Voyage of Guangzhou Basic and Applied Basic Research Scheme (Grant No. 2024A04J4186). We thank the Semiconductor and Nano-Technology Center of Guangdong University of Technology for providing the cleanroom and characterization facilities. We acknowledge the Shanghai Synchrotron Radiation Facility (SSRF) for providing the beamtime and technical support.

Conflict of Interest

The authors declare no conflict of interest.

Data Availability Statement

The data that support the findings of this study are available from the corresponding author upon reasonable request.

Keywords

Single pulse all-optical switching, Ultrafast spin dynamics, Interlayer exchange coupling, Two-sublattice ferrimagnet dynamics

References

1 Stanciu, C. D. *et al.* All-optical magnetic recording with circularly polarized light. *Phys Rev Lett* **99**, 047601 (2007). https://doi.org/10.1103/PhysRevLett.99.047601

2 Strungaru, M. *et al.* All-Optical Switching: A Path to Recording Technology Beyond HAMR. *IEEE Transactions on Magnetics* **61**, 1-9 (2025). https://doi.org/10.1109/tmag.2025.3530769

3 Stupakiewicz, A., Szerenos, K., Afanasiev, D., Kirilyuk, A. & Kimel, A. V. Ultrafast nonthermal photo-magnetic recording in a transparent medium. *Nature* **542**, 71-74 (2017). https://doi.org/10.1038/nature20807

4 Lu, X. Y. *et al.* Roles of heating and helicity in ultrafast all-optical magnetization switching in TbFeCo. *Applied Physics Letters* **113**, 032405 (2018). https://doi.org/https://doi.org/10.1063/1.5036720

5 Remy, Q. *et al.* Energy Efficient Control of Ultrafast Spin Current to Induce Single Femtosecond Pulse Switching of a Ferromagnet. *Adv Sci (Weinh)* **7**, 2001996 (2020). https://doi.org/10.1002/advs.202001996

6 Mangin, S. *et al.* Engineered materials for all-optical helicity-dependent magnetic switching. *Nat Mater* **13**, 286-292 (2014). https://doi.org/10.1038/nmat3864

7 Lambert, C. H. *et al.* All-optical control of ferromagnetic thin films and nanostructures. *Science* **345**, 1337-1340 (2014). https://doi.org/10.1126/science.1253493

8 Zhang, P. *et al.* All-optical switching of magnetization in atomically thin CrI(3). *Nat Mater* **21**, 1373-1378 (2022). https://doi.org/10.1038/s41563-022-01354-7

9 Da Browski, M. *et al.* All-optical control of spin in a 2D van der Waals magnet. *Nat Commun* **13**, 5976 (2022). https://doi.org/10.1038/s41467-022-33343-4

10 Ellis, M. O., Fullerton, E. E. & Chantrell, R. W. All-optical switching in granular ferromagnets caused by magnetic circular dichroism. *Sci Rep* **6**, 30522 (2016). https://doi.org/10.1038/srep30522

11 Chen, J.-Y., He, L., Wang, J.-P. & Li, M. All-Optical Switching of Magnetic Tunnel Junctions with Single Subpicosecond Laser Pulses. *Physical Review Applied* **7** (2017). https://doi.org/10.1103/PhysRevApplied.7.021001

12 Ceballos, A. *et al.* Role of element-specific damping in ultrafast, helicity-independent, all-optical switching dynamics in amorphous (Gd,Tb)Co thin films. *Physical Review B* **103** (2021). https://doi.org/10.1103/PhysRevB.103.024438

13 Khorsand, A. R. *et al.* Role of magnetic circular dichroism in all-optical magnetic recording. *Phys Rev Lett* **108**, 127205 (2012). https://doi.org/10.1103/PhysRevLett.108.127205

14 Lalieu, M. L. M., Peeters, M. J. G., Haenen, S. R. R., Lavrijsen, R. & Koopmans, B. Deterministic all-optical switching of synthetic ferrimagnets using single femtosecond laser pulses. *Physical Review B* **96** (2017). https://doi.org/https://doi.org/10.1103/PhysRevB.96.220411

15 Alebrand, S. *et al.* Light-induced magnetization reversal of high-anisotropy TbCo alloy films. *Applied Physics Letters* **101** (2012). https://doi.org/10.1063/1.4759109

16 Banerjee, C. *et al.* Single pulse all-optical toggle switching of magnetization without gadolinium in the ferrimagnet Mn2RuxGa. *Nat Commun* **11**, 4444 (2020). https://doi.org/10.1038/s41467-020-18340-9

17 Igarashi, J. *et al.* Optically induced ultrafast magnetization switching in ferromagnetic spin valves. *Nat Mater* (2023). https://doi.org/10.1038/s41563-023-01499-z

18 Radu, I. *et al.* Transient ferromagnetic-like state mediating ultrafast reversal of antiferromagnetically coupled spins. *Nature* **472**, 205-208 (2011). https://doi.org/10.1038/nature09901

19 Ostler, T. A. *et al.* Ultrafast heating as a sufficient stimulus for magnetization reversal in a ferrimagnet. *Nat Commun* **3**, 666 (2012). https://doi.org/10.1038/ncomms1666

20 Davies, C. S. *et al.* Pathways for Single-Shot All-Optical Switching of Magnetization in Ferrimagnets. *Physical Review Applied* **13** (2020). https://doi.org/10.1103/PhysRevApplied.13.024064

21 Boeglin, C. *et al.* Distinguishing the ultrafast dynamics of spin and orbital moments in solids. *Nature* **465**, 458-461 (2010). https://doi.org/10.1038/nature09070

22 Dornes, C. *et al.* The ultrafast Einstein-de Haas effect. *Nature* **565**, 209-212 (2019). https://doi.org/10.1038/s41586-018-0822-7

23 Remy, Q. *et al.* Accelerating ultrafast magnetization reversal by non-local spin transfer. *Nat Commun* **14**, 445 (2023). https://doi.org/10.1038/s41467-023-36164-1

24 Malinowski, G. *et al.* Control of speed and efficiency of ultrafast demagnetization by direct transfer of spin angular momentum. *Nature Physics* **4**, 855-858 (2008). https://doi.org/10.1038/nphys1092

25 A. V. Kimel, A. K., A. Tsvetkov, R. V. Pisarev & Th. Rasing Laser-induced ultrafast spin reorientation in the antiferromagnet TmFeO3. *Nature* **429**, 848-850 (2004). https://doi.org/10.1038/nature02609

26 Kunyangyuen, B. *et al.* Controlling Single-Pulse Magnetization Switching through Angular Momentum Reservoir Engineering. *ACS Materials Letters* **7**, 3619-3625 (2025). https://doi.org/10.1021/acsmaterialslett.5c01060

27 Ruderman, M. A. & Kittel, C. Indirect exchange coupling of nuclear magnetic moments by conduction electrons. *Physical Review* **96**, 99 (1954).
28 Kasuya, T. Prog. Theor. Phys. *Prog. Theor. Phys.* **16**, 45 (1956).
29 Kastler, A. Optical methods of atomic orientation and of magnetic resonance. *JOSA* **47**, 460-465 (1957).
30 Yosida, K. Magnetic properties of Cu-Mn alloys. *Physical Review* **106**, 893 (1957).
31 Kresse, G. & Hafner, J. Ab initio molecular dynamics for open-shell transition metals. *Physical Review B* **48**, 13115 (1993).
32 Kresse, G. & Furthmüller, J. Efficient iterative schemes for ab initio total-energy calculations using a plane-wave basis set. *Physical review B* **54**, 11169 (1996).
33 Rhee, I. *et al.* Shift of Curie Temperature in Gadolinium Films\due to Finite-Size Effects. *Journal of the Physical Society of Japan* **64**, 678-679 (1995).
34 Yamada, Y., Okada, M., Jin, P., Tazawa, M. & Yoshimura, K. The Curie temperature dependence on preparation conditions for Gd thin films. *Thin Solid Films* **459**, 191-194 (2004).
35 Lalieu, M. L. M., Lavrijsen, R. & Koopmans, B. Integrating all-optical switching with spintronics. *Nat Commun* **10**, 110 (2019). https://doi.org/10.1038/s41467-018-08062-4
36 Yang, Q. *et al.* Ionic liquid gating control of RKKY interaction in FeCoB/Ru/FeCoB and (Pt/Co)2/Ru/(Co/Pt)2 multilayers. *Nat Commun* **9**, 991 (2018). https://doi.org/10.1038/s41467-018-03356-z
37 Leon, A. O., d'Albuquerque e Castro, J., Retamal, J. C., Cahaya, A. B. & Altbir, D. Manipulation of the RKKY exchange by voltages. *Physical Review B* **100** (2019). https://doi.org/10.1103/PhysRevB.100.014403
38 Kim, K., Jang, S., Shin, K., Kim, H. & Kang, T. Interlayer coupling field in spin valves with CoFe/Ru/CoFe/FeMn synthetic antiferromagnets. *Journal of Applied Physics* **89**, 7612-7615 (2001).
39 Blasing, R. *et al.* Exchange coupling torque in ferrimagnetic Co/Gd bilayer maximized near angular momentum compensation temperature. *Nat Commun* **9**, 4984 (2018). https://doi.org/10.1038/s41467-018-07373-w
40 Hintermayr, J., Ullrich, A. & Albrecht, M. Structure and magnetic properties of ferrimagnetic [Gd/Fe]n multilayer and GdxFe100−x thin films. *AIP Advances* **11** (2021). https://doi.org/10.1063/5.0057667
41 Hellman, F. *et al.* Interface-Induced Phenomena in Magnetism. *Rev Mod Phys* **89**, 025006 (2017). https://doi.org/10.1103/RevModPhys.89.025006
42 Ostler, T. *et al.* Ultrafast heating as a sufficient stimulus for magnetization reversal in a ferrimagnet. *Nature communications* **3**, 666 (2012).
43 Barker, J. *et al.* Two-magnon bound state causes ultrafast thermally induced magnetisation switching. *Sci Rep* **3**, 3262 (2013). https://doi.org/10.1038/srep03262
44 Evans, R. F. *et al.* Atomistic spin model simulations of magnetic nanomaterials. *Journal of Physics: Condensed Matter* **26**, 103202 (2014).
45 Ceballos, A. *et al.* Role of element-specific damping in ultrafast, helicity-independent, all-optical switching dynamics in amorphous (Gd, Tb) Co thin films. *Physical Review B* **103**, 024438 (2021).

Supplementary Files

This is a list of supplementary files associated with this preprint. Click to download.

- Supportinginformation.docx